PCCP

Semicoordinate and Halogen Bonding to Group 10 and Group 8 Metals

Journal:	*Physical Chemistry Chemical Physics*
Manuscript ID	CP-ART-05-2025-001662.R1
Article Type:	Paper
Date Submitted by the Author:	24-May-2025
Complete List of Authors:	Scheiner, Steve; Utah State University, Department of Chemistry and Biochemistry

SCHOLARONE™
Manuscripts

Semicoordinate and Halogen Bonding to Group 10 and Group 8 Metals

Steve Scheiner*

Department of Chemistry and Biochemistry
Utah State University
Logan, Utah 84322-0300
USA

*email: steve.scheiner@usu.edu

Abstract

A series of square planar systems are constructed, placing a Group 10 metal atom at the center, connected to two ditopic ligands by four M-S bonds. DFT calculations show that the metal can form a noncovalent bond with an approaching NH_3 ligand, with a strength that varies from 10.8 kcal/mol for Ni, down to 1.8 kcal/mol for Pt. This pattern conforms to the charge on the M which reverses from positive to negative in this same order. A XCCH molecule (X=I,Cl) can approach the metal system in a perpendicular configuration. Although this geometry suggests halogen bonding through electron donation from M to the X σ-hole, detailed scrutiny of the electronic structure shows the strongest element to be noncovalent semicoordinate bonding, involving charge transfer from X lone pairs to M. Other stable configurations place the XCCH unit parallel to the metal system, also held together by a semicoordinate bond. Group 8 metals form a shorter and stronger covalent bond with NH_3. While Os forms perpendicular arrangements with XCCH, Fe and Ru do not.

Keywords: Charge transfer; noncovalent bond; NBO; electrostatic potential; SAPT

INTRODUCTION

The H-bond is arguably the most important of all noncovalent interactions, figuring prominently in a diverse range of chemical and biological phenomena such as solvation, genetic replication, and enzymatic activity [1-9]. Recent years have brought to the fore a class of closely related noncovalent bonds wherein the bridging proton is replaced by any of a large set of other atoms, mainly drawn from the right side of the periodic table [10-19]. Although these interactions do not have the advantage of a positive H atom to attract a nucleophile, they rely instead on a restricted region of positive electrostatic potential that lies along the extension of the covalent bond which connects this bridging atom to the Lewis acid molecule. This region of positive charge, attributed to a deficiency of electron density, has been termed a σ-hole [20, 21] and thus the associated bonds are classified as σ-hole bonds. In a more general sense, there are situations where the positive region lies not along a bond axis, but rather above the plane of the molecule, and is thus referred to as a π-hole [22-26].

It is common to subclassify these bonds according to the family of the periodic table from which the bridging atom is derived, thus leading to the halogen, chalcogen, pnicogen, tetrel, and triel bonds that have found their way into common chemical parlance. Their importance is undeniable, as their strength is comparable to the H-bond, exceeding it in many instances. Like the H-bond, these bonds too are major players in widespread chemical phenomena such as catalysis, supramolecular structure, self-assembly, and ion transport [27-34]. Intensive study of these interactions in recent years has led to a great deal of information and insights concerning their fundamental nature, their strength, and the way in which they are modified by both the identity of the bridging atom and any of its substituents.

There is of course no reason that these bridging atoms must be limited to the p-block elements on the right side of the periodic table. One might conjecture that the transition metals of the d-block, with their greater electropositivity, ought to present σ and π-holes that are even more positive than the non-metallic atoms to their right, and perhaps then stronger interactions with a nucleophile. And in fact, the recent literature has sprung to life with a rapidly increasing number of tentative observations of interactions that have all the markings of bonds of this sort. In the spirit of the p-block family, these bonds are often named after the particular column of the periodic table. Those involving Group 12 metals have been christened spodium bonds [35-42] and those including Group 11 go by the moniker of either regium or coinage metal bonds [43-50]. Osme bonds encompass Group 8, [51, 52], matere bonds arise from Group 7 [53-57], wolfium bonds denote Group 6 [58, 59], and erythronium bonds correspond to Group 5 [60].

There has been a significant amount of attention turned recently to the Ni/Pd/Pt group 10 metals as well. Some work addressed clusters of these and other metal atoms and found that their catalytic activity is guided by the positioning of their σ-hole maxima [61-64]. In the context of smaller and more common occurrences, these atoms frequently appear within a square planar configuration, leaving a vacancy directly above the plane to which ligands can attach [65-72]. In many cases, the d_z2 orbital serves as a reservoir of electron density to which an electrophile might attach, perhaps forming a halogen bond [73].

One work [74] had considered Ni in a square planar coordination within a nitrosoguanidinate complex $Ni\{NH=C(NMe_2)\text{-}NN(O)\}_2$ and related systems. Upon cocrystallization with I_2 and related systems, the authors noted the I_2 could approach the Ni end-on, such that the I σ-hole might accept charge from a Ni d_z2 orbital, in an apparent halogen bond. But an alternate arrangement rotates the I_2 by roughly 90°, which sets up charge transfer from the I lone pairs to the Ni. As such, these results emphasized what the authors dubbed the electrophilic-nucleophilic dualism of Ni. Soon thereafter, Zelenkov et al [75] broadened this idea to other metals, focusing in particular on several $M^{II}(S_2CNEt_2)_2$ dithiocarbamate complexes, where M refers to any of the group 10 metals, as well as Cu, in a square planar setting. Crystals were grown in which I atoms of neighboring molecules approached the M atom from above in what had the geometric appearance of CI··M halogen bonds. Their work again suggested that a rotation of the I-containing ligand presents the I lone pairs toward the M, switching the role of electron donor and acceptor. While these works did indeed find computational indications of M··I bonding in the perpendicular complexes, they did not fully probe the question of the true nature of this bonding, assuming it to be halogen bonding based on geometries.

A more comprehensive computational study soon thereafter [76] of the group 10 metals within a similar square planar situation found that both a nucleophile such as pyridine, and an apparent electrophilic C_6F_5I can approach the M atom from directly above so as to form a stable complex. The latter did indeed show some evidence of CI··M halogen bonding in that a certain amount of charge was transferred from the M lone pair to the σ*(CI) antibonding orbital. However, these workers did not consider if there were any transfer in the reverse direction, from the I lone pairs to the M center. Such a transfer, if present, would be indicative of an entirely different sort of bonding in which it is the M that plays the role of electron acceptor. In fact, there are some indications that this might be the case, based on very recent calculations of other planar metal systems [77].

And indeed, the calculations presented below demonstrate this to be true for the entire set of group 10 metals, and that these bonds would be better classified as transition metal, or semicoordinate bonds, rather than halogen bonds. The data shows this categorization applies to the full range of group 10 metals, whether the M carries a partial positive (Ni) or negative (Pt) charge. The calculations also find additional stable complexes, other than perpendicular, where the ligand is turned so that it presents the halogen lone pairs toward the M, rather than its σ-hole. The M atom again plays the role of electrophile here, accepting charge from the halogen lone pairs. As such, it might be misleading to discuss the bonding of these metals in the context of electrophilic-nucleophilic dualism since the central metal acts primarily as electrophile, regardless of the orientation of the ligand. The work described below goes on to explore the extension of the findings to other transition metals, in this case comparing group 10 with group 8 metals, finding some significant distinctions.

METHODS

The Gaussian 16 [78] suite of programs was employed to carry out the quantum chemical calculations, applying the DFT M06-2X functional [79] in conjunction with the triple-ζ def2-TZVP basis set. A relativistic pseudopotential is incorporated into this basis for the heavier 5d metal atoms. M06-2X has been repeatedly assessed to be one of the most accurate functionals for H-bonding and related noncovalent interactions [80-88]. Geometries were fully optimized, and characterized as true minima by harmonic vibrational analysis which yielded all positive frequencies, unless indicated otherwise. The interaction energy E_{int} is equal to the difference between the energy of the dyad and the sum of the energies of the two monomers in the geometry they adopt within the complex; E_{int} was corrected for basis set superposition error by the standard counterpoise prescription [89].

The Multiwfn program [90] located and quantified the maxima of the molecular electrostatic potential (MEP) on the ρ=0.001 au isodensity surface of each isolated monomer. Atoms in Molecules (AIM) bond paths and the properties of their associated critical points were evaluated via the AIMAll program [91]. NBO analysis of interorbital charge transfer [92, 93] was carried out via the NBO routines incorporated into the Gaussian package. Interaction energies were decomposed into their various components via symmetry-adapted perturbation theory (SAPT) [94, 95] via the Psi4 program [96].

RESULTS

In keeping with recent experimental work [75], the metal-bearing systems each placed M within a square planar arrangement surrounded by four M-S bonds. The M center is held in this configuration by a pair of ditopic S(CH)S ligands, as pictured in Fig 1. In addition to the three group 10 metals in the top row of Fig 1, their group 8 congeners Fe, Ru, and Os in the bottom row were considered as well, for purposes of comparison.

Monomer Properties

One property of each molecule of major importance is the molecular electrostatic potential (MEP) surrounding it. This MEP is illustrated in Fig 1 for each molecule, and they all share a negative (red) region around the S atoms, while the blue areas near the CH groups designate a positive MEP. Of particular interest is the region directly above each metal center. The MEP is light blue for the 3d metals Ni and Fe, then becomes red as one moves down in the periodic table. This progression from positive to negative is quantified by V_{max}, the maximum in the MEP on the 0.001 au isodensity surface. As is evident in Table 1, this quantity is positive for Ni and Fe, then quickly turns negative for the heavier M atoms in each column. Another measure of the potential near the metal atom is its natural atomic charge. These quantities are compiled on the right side of Table 1. The results echo the MEP in that the charge on the lightest metal of each group is positive, while the others are negative. Unlike V_{max}, the charges suggest the 4d metals Pd and Ru are slightly more negative than their 5d analogues, but only by a small amount.

A second important element of the electronic structure can be visualized by an ELF diagram which locates regions of electron pair density. Fig 2a depicts the ELF diagram of the planar Pt system and the corresponding picture for the Group 8 Os system is contained in Fig 2b. The diagrams of the other systems all closely resemble those in Fig 2. It is clear that both Group 10 and 8 metal atoms exhibit a vacancy of electron pair density directly above the M center. This

opening could create an opportunity for the approach of an electron pair of a nucleophile, an opportunity which is exploited by the various ligands as discussed below.

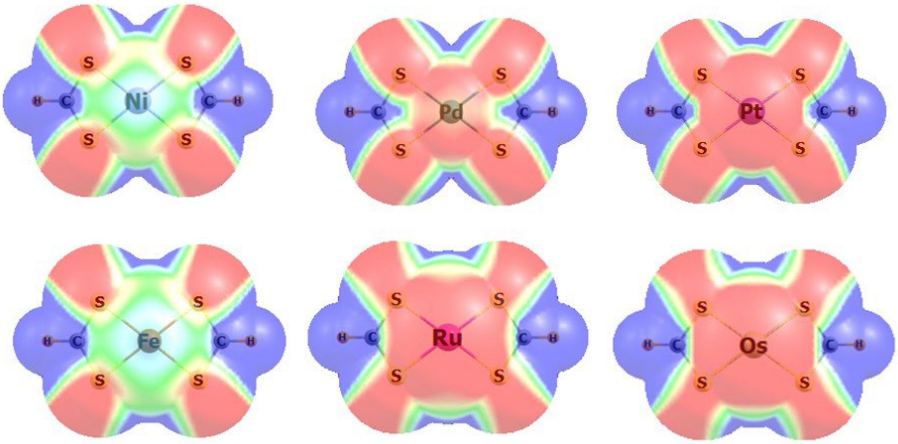

Fig 1. Molecular electrostatic potential surrounding metal systems. Blue and red regions respectively denote positive and negative MEP, corresponding to ±3 kcal/mol.

Table 1. V_{max} lying directly above M atom, and natural charge on M.

	V_{max}, kcal/mol				q_M, e			
	Group 10		Group 8		Group 10		Group 8	
3d	Ni	+13.2	Fe	+14.0	Ni	+0.293	Fe	+0.230
4d	Pd	-0.3	Ru	-4.4	Pd	-0.048	Ru	-0.265
5d	Pt	-8.4	Os	-9.6	Pt	-0.031	Os	-0.192

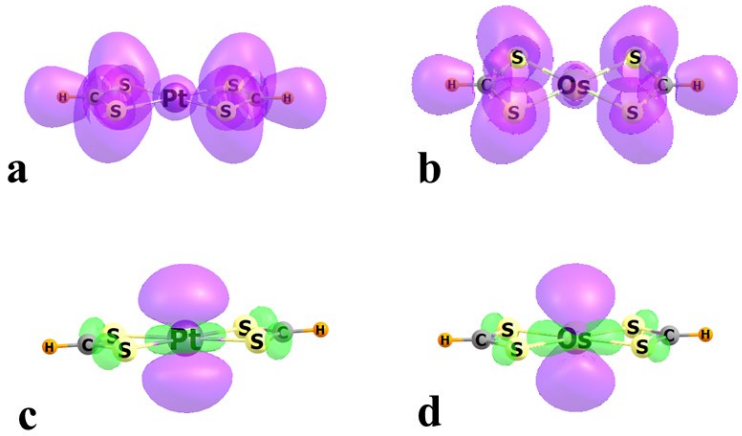

Fig 2. ELF diagrams of a) Pt and b) Os systems. Occupied orbitals of c) Pt and d) Os systems that can overlap with and transfer charge to approaching electrophile.

The positive MEP above the 3d metal centers ought to provide a particularly welcoming environment for a nucleophile. This approach might be inhibited, however, by the negative MEP above the heavier metal atoms. From the opposite perspective, the approach of an electrophile

might be encouraged by the negative potentials above these heavier metals. One example of such an electrophile might be the halogen (X) atom on XCCH. The positive charge associated with the X σ-hole could be attracted by the negative M centers, facilitating the formation of a M··X halogen bond. The charge transfer into the σ*(XC) antibonding orbital could arise from either the d_z2 orbital of the metal or from any of the M-S bonding orbitals, all of which are well disposed to interact with σ*(XC). The relevant MOs are pictured in Fig 2c and 2d for the Pt and Os monomers. There is clearly an occupied orbital on the metal center which could overlap nicely with an approaching electrophile so as to engage in a halogen bond. So it would appear that these systems are disposed to interact with either a nucleophile or electrophile, consistent with the idea of electrophilic-nucleophilic dualism suggested earlier.

Type 1 M··N Dyads

The first sort of interaction considers NH_3 as a prototype electron donor, via its N lone pair. As illustrated in Fig 3, dyad 1 places the N directly above the metal center, Pt in the case shown. The salient properties of each such type 1 complex are collected in Table 2. There is first a clear distinction between the dyads with Group 10 and 8 metals. The latter form very strong bonds, with interaction energies surpassing 30 kcal/mol, and with short R(M··N) distances of 2.0 Å. The density of the intermolecular bond critical point is quite large, between 0.067 and 0.107 au, all suggesting a bond of largely covalent character.

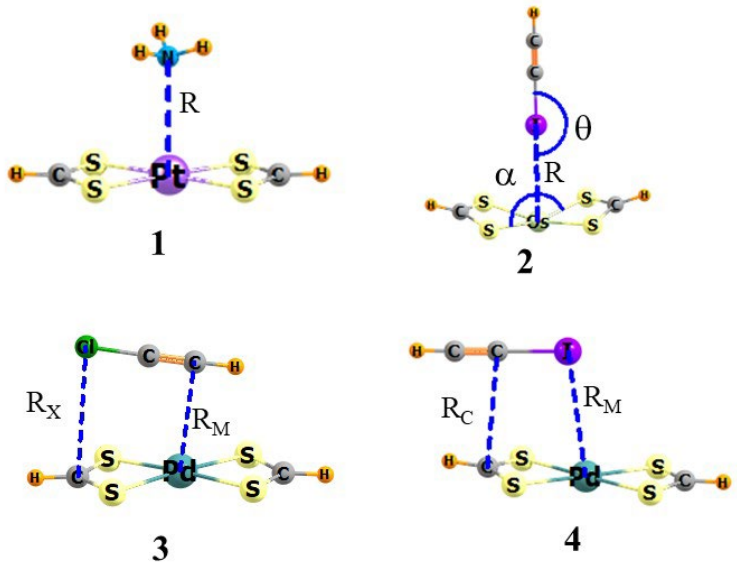

Fig 3. Dispositions of two subunits in various dimer types, defining geometrical parameters.

The group 10 metals, on the other hand, form much weaker bonds with NH_3. The interaction energies are 10 kcal/mol or less, and they weaken as the metal atom grows larger. This trend mirrors the progressively more negative potential on the M atom, which would be less accommodating to the nucleophile. The weakening bond is characterized also by a progressively longer M··N separation. This distance, between 2.43 and 3.11 Å is much longer than the coordinate covalent bonds of the Group 8 series. Also much smaller is the BCP density, which drops from a maximum of 0.035 au for Ni down to only 0.016 au for Pt, all in the range expected for a noncovalent bond. Along with the longer distances is a reducing amount of charge transferred from NH_3 to the metal system, in the 45-96 me range. The last row of Table 2 lists

the NBO second-order perturbation energy E2 connected with the transfer from the N lone pair to the orbital characterized by NBO to be an empty lone pair orbital on M. The strong overlap between these two orbitals that facilitates this transfer is visualized in Fig 4a for the Pt system. Examination of this orbital reveals it to be an empty p_z-orbital. Note that such a transfer is not pertinent to most of the type 1 dyads as NBO views the complex as a single molecular unit.

Table 2. Properties of type 1 complexes with NH_3. CT refers to total charge transferred from NH_3 to metal system as sum of natural charges on each subunit.

	Ni	Pd	Pt	Fe	Ru	Os
$-E_{int}$, kcal/mol	10.79	4.53	1.78	43.73	41.04	33.40
R, Å	2.426	2.836	3.111	2.049	2.073	2.070
ρ, 10^{-4} au	354	218	158	669	951	1069
CT, me	96	63	45	245	369	335
E2($N_{lp}\rightarrow Mp_z^*$), kcal/mol	a	24.8	15.1	a	a	a

[a] NBO considers complex as single unit

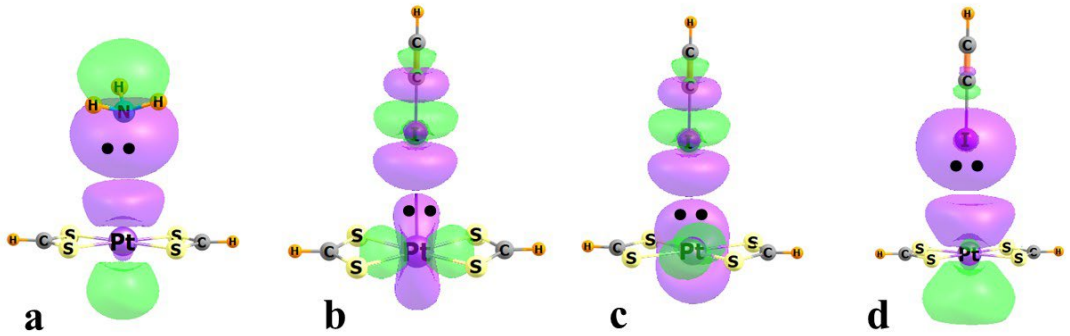

Fig 4. Orbital overlaps between two subunits. a) lone pair of N with vacant p_z orbital of Pt. b,c) occupied d-orbitals of Pt with σ*(CI) orbital of ICCH. d) occupied I lone pair with vacant p_z orbital of Pt.

The upper segment of Table 3 lists the SAPT components of the interaction energy for the noncovalent bonds of group 10 metals. It is immediately clear that the electrostatic element ES drops drastically as M grows larger and more negative. The percentage contribution of ES to the sum of the three attractive terms diminishes as well. While ES makes up 65% of this sum for Ni with its positive charge, its contribution drops to only 37% for Pt. The magnitudes of the induction energy (IND) and dispersion (DISP) also diminish in this same order, but much of that can be tied to rapidly elongating intermolecular separation.

In summary, NH_3 forms a strong coordinate covalent bond with the group 8 metals, but a much weaker noncovalent bond with the metals of group 10. The latter are quite dependent upon the size and charge of M, dropping from 10.8 to 1.8 kcal/mol as V_{max} on Pt becomes significantly negative in sign. Importantly, the negative MEP on the heavier M atoms does not preclude the formation of this bond, even if it does weaken it.

Table 3. SAPT components (kcal/mol) of interaction energies of dyads with group 10 metals, and their percentage contribution to the total of the three attractive elements.

	ES	IND	DISP	EX	%ES	%IND	%DISP
1 NH_3							
Ni	-27.97	-6.48	-8.91	29.93	64.5	14.9	20.6
Pd	-9.31	-2.96	-6.26	13.23	50.3	16.0	33.8
Pt	-4.04	-2.03	-4.93	8.91	36.7	18.5	44.8
2 ICCH							
Ni	-6.45	-2.51	-8.92	6.45	36.1	14.0	49.9
Pd	-1.55	-1.58	-7.58	6.80	14.5	14.7	70.8
Pt	-3.72	-2.18	-8.55	8.67	38.2	10.9	50.9
3 ICCH							
Ni	-8.06	-2.44	-11.51	11.51	36.6	11.1	52.3
Pd	-5.08	-1.56	-10.54	11.30	29.6	9.1	61.3
Pt	-3.96	-1.31	-9.67	9.79	26.5	8.8	64.7
4 ICCH							
Ni	-6.44	-2.05	-10.66	13.09	33.6	10.7	55.6
Pd	-4.72	-1.42	-10.03	10.56	29.2	8.8	62.0
Pt	-4.29	-1.29	-9.42	9.72	28.6	8.6	62.8

Perpendicular Type 2 Dyads

In a reversal of the case in type 1, where the partner NH_3 molecule approaches M with its lone electron pair forward, along with its negative charge, it is the density depleted, positively charged σ-hole of the halogen X atom of XCCH (X= I, Cl) that leads the way toward M in geometries of type 2. An example of such an arrangement is depicted in Fig 3b for ICCH and the Os system, which also defines the angular aspects of this dyad. As a prelude, given the electron-deficient nature of the XCCH, one would expect a bonding advantage for a negatively charged M center.

Table 4. Properties of type 2 complexes with XCCH. CT refers to total charge transferred from XCCH to metal system.

	Ni-I	Pd-I	Pt-I	Pt-Cl[a]	Os-I	Os-Cl
$-E_{int}$	4.61	3.68	4.56	2.23	4.99	2.57
R	3.391	3.465	3.469	3.364	3.652	3.556
θ	122.6	175.0	179.9	180.0	180.0	180.0
α	178.8	178.5	179.1	178.9	165.2	163.7
ρ	121	107	128	103	114	90
CT	29	15	28	22	12	13
$E2(X_{lp} \rightarrow Mp_z^*)$	10.0	10.5	21.5	14.7	16.8	11.0
$E2(M_{lp} \rightarrow \sigma^*_{XC})$	1.9	2.7	3.4	1.7	3.6	1.3

[a]small imaginary frequency of 4i cm^{-1}

The most important characteristics of these type 2 complexes are compiled in Table 4. It might first be underscored that not all pairs yield a stable geometry of this sort. For example, of the group 8 metals, it is only Os that engages with either ICCH or ClCCH. All of the group 8

metals form a type 2 structure with ICCH, but ClCCH can engage only with Pt. While one might expect a linear geometry, with both θ and α nearly equal to 180°, and this is indeed the case for most, θ is markedly nonlinear for Ni and α deviates by 15° for the two Os structures.

The interaction energies in Table 4 lie in the range between 2.2 and 5.0 kcal/mol. Those involving Cl are both weaker than the corresponding I complexes. This disparity is an expected one for halogen bonds, based in part on the shallower σ-hole of Cl. Regarding the M-I dyads, there is an ordering of Os > Ni ~ Pt > Pd. Like E_{int}, the BCP densities are also fairly similar, all around 0.01 au, placing them in the noncovalent category.

Inspection of the charge transfers in the next row of Table 4 reveals an unexpected finding. Whereas one would expect charge in a halogen bond to flow from the metal complex to XCCH, the opposite is found. The positive CT quantities in Table 4 are consistent with an overall transfer from XCCH. The next two rows of the table help explain this surprising finding. The final row reports E2 for the transfer into the XC antibonding orbital, typical of a halogen bond. This charge originates in various orbitals including the M lone pairs and the π(MS) bonding orbitals. The overlap between two of these Pt lone pairs and the σ*(IC) orbital is exhibited in Fig 4b and 4c. While this quantity is significant, it is swamped by a much larger E2 associated with transfer in the opposite direction, from the lone pairs of the X atom into the empty p_z orbital of the metal center. The relevant pair of orbitals are depicted in Fig 4d. From this diagram, it may be seen that the orbital alignments that facilitate this latter transfer are only slightly affected by the aforementioned nonlinearities in θ and α, helping to explain these geometries.

The breakdown of the interaction energies for the type 2 dyads in the second segment of Table 3 paints a somewhat different profile than for the type 1 geometries. In the first place, the ES contributions are considerably smaller. As a consideration regarding ES, recall that the metal atoms become progressively less positive/more negative in the progression from Ni to Pt. Since this metal is directly facing the positive σ-hole of the incoming ICCH, one would expect a more stabilizing ES in the same order. Yet Table 3 shows that it is the Ni that has the most stabilizing ES, despite its positive charge. Note from Table 2 that it is this same Ni complex where θ deviates by 57° from linearity. This rotation of the ICCH molecule can be understood on the basis of alleviating the coulombic repulsion between the I σ-hole and the positive charge of the Ni center. Other than ES, there are only minor variations in the other components of the type 2 structures. Overall, these complexes are highly dependent upon dispersion, which accounts for between 50% and 70% of the total attractive energy.

So in summary, while the type 2 complexes do indeed contain a significant degree of halogen bonding, they are more dependent on noncovalent bonding wherein the X lone pairs serve as electron donors to the metal system. It would be easy to be misled that the interaction is dominated by halogen bonding by the geometry. This misconception might be reinforced by the observation that the CI bond of ICCH undergoes a stretch, by 0.004, 0.006, and 0.010 Å upon complexation with the Ni, Pd, and Pt systems, respectively. It requires a deeper dive into the specific orbital interactions and overall charge transfer direction to reveal that while there is a certain element of halogen bonding to be sure, it is the interaction between the X lone pairs and the M unoccupied orbitals that provides the chief element in the bonding picture. From an electrostatic point of view, the charge on the M atom shifts from positive to negative in the Ni→Pd→Pt sequence, so one would expect a progressively more favorable coulombic interaction with the X σ-hole, and thus a stronger interaction in this order. Yet the interaction energies are fairly insensitive to the identity of the metal. Indeed, it is Ni, with its positive charge, that forms the strongest bond with ICCH. As another perspective, one measure of the

transition metal (TM) π-hole bonding is the charge loss from the X lone pairs, coupled with that gained by the M p_z* orbital. Taking Pt-I as an example, these quantities are 0.044 and 0.039 e, respectively. A halogen bond, on the other hand, would involve transfer into the σ*(CI) antibonding orbital. This quantity is only 0.019 e, much less than that measuring the Pt π-hole bonding.

Type 3 and 4 Parallel Structures

A completely different geometry was also identified as a minimum for those systems containing Ni, Pd, Pt and Os. This structure 3 is held together by two separate bonds as the XCCH aligns itself nearly parallel to the metal systems, as illustrated in Fig 3. There is an AIM bond path leading from the central M to the C atom of the CH group, while the X center of XCCH is the terminus of another bond path to one of the C atoms of the M system. The two bondlengths are listed in Tables 5 and 6, along with the BCP densities, and the overall interaction energy. In most cases R_M is shorter than R_X, suggesting the former to be a stronger bond, particularly in the face of the large size of the M atom. This idea is borne out by the larger ρ_{BCP} for the former, roughly twice the magnitude of the latter. These R(M··C) distances are also substantially shorter than the R(M··X) quantities for type 2 listed in Table 4.

Table 5. Properties of type 3 complexes of group 10 metals with XCCH. M and X subscripts respectively indicate the M··C and X··C bond paths. CT refers to total charge transferred from XCCH to metal system.

	Ni-I	Pd-I	Pt-I	Ni-Cl	Pd-Cl	Pt-Cl
$-E_{int}$	5.97	4.44	3.44	5.65	4.11	3.13
R_M	2.965	3.159	3.323	2.963	3.157	3.347
R_C	3.741	3.784	3.751	3.515	3.542	3.454
ρ_M	128	116	100	128	116	97
ρ_X	61	57	57	61	57	60
CT	17	19	22	19	21	22
$\pi(CC)\rightarrow Mp_z$*	4.2	4.1	4.2	5.3	5.4	3.9
$X_{lp}\rightarrow SC$	0.9	0.9	1.2	0.6	0.6	1.0

Table 6. Properties of type 3 complexes of group 8 metals with XCCH. M and X subscripts respectively indicate the M··C and X··C bond paths. CT refers to total charge transferred from XCCH to metal system.

	Fe-I	Os-I	Fe-Cl	Os-Cl[a]
$-E_{int}$	6.01	2.97	5.56	2.67
R_M	2.993	3.555	3.000	3.584
R_X	3.810	3.780	3.566	3.470
ρ_M	139	81	139	78
ρ_X	57	55	56	58
CT	18	12	21	12
$\pi(CC)\rightarrow Mp_z$*	6.0	2.3	6.9	0.8
$X_{lp}\rightarrow SC$	0.6	1.0	0.4	0.8

[a]small imaginary frequency of 14i cm^{-1}

There is a clear pattern in the energetics of these complexes in Table 4. The interaction energies decrease in the order Ni > Pd > Pt in roughly 1 kcal/mol decrements, and R_M elongates in this same order. There is a small decrement of 0.3 kcal/mol in switching out I for the smaller Cl halogen center. The group 8 systems in Table 6 agree in the diminishing interaction energies and bond strength as one moves down in that periodic table column. There is also a near equality in the Ni/Fe and Pt/Os interaction energies. But it is notable that Ru does not form a type 3 complex.

The CT row of Tables 5 and 6 reports the total charge that is transferred from the XCCH molecule to the M system. These quantities lie in the range between 12 and 22 me. Analysis of the NBO treatment of these type 3 complexes offers clues as to the source of the transfer. There are two chief elements of transfer, and both in the same direction from XCCH to the metal system. The first and larger of the two shifts charge from the C≡C π-bonding orbitals to the empty p_z orbital of M. The second and smaller shift occurs from the X lone pairs to the SC antibonding orbitals in what might be termed a tetrel bond. So the type 3 dimers are stabilized primarily by a π-hole, with a weaker tetrel bond as a supplement.

The parallel alignment of the two systems in complex 3 is highly conducive of a large dispersion component, which is indeed confirmed by the third segment of Table 3. The dispersion energy is quite large, between 10 and 12 kcal/mol, and accounts for more than half of the total interaction energy. Second in importance is ES, at roughly 30%. Induction energy is much smaller, only around 10%.

Table 7. Properties of type 4 complexes of group 10 metals with XCCH. M and C subscripts respectively indicate the M··X and C··C bond paths. CT refers to total charge transferred from XCCH to metal system.

	Ni-I	Pd-I	Pt-I	Ni-Cl	Pd-Cl	Pt-Cl
$-E_{int}$	5.13	4.21	3.65	3.85	3.15	2.88
R_M	3.417	3.645	3.890	3.175	3.524	3.764
R_C	3.407	3.465	3.322	3.423	3.314	3.277
ρ_M	121	105	82	115	82	64
ρ_C	58	61	64	57	64	66
CT	52	51	47	32	25	25
$X_{lp}\rightarrow Mp_z^*$	11.1	15.5	17.3	7.4	8.0	8.7

Table 8. Properties of type 4 complexes of group 8 metals with XCCH. M and C subscripts respectively indicate the M··X and C··C bond paths. CT refers to total charge transferred from XCCH to metal system.

	Fe-I	Ru-I[b]	Os-I	Fe-Cl	Ru-Cl[a]	Os-Cl[a]
$-E_{int}$	4.64	3.47	3.19	3.49	2.73	2.61
R_M	3.418	3.942	4.114	3.303	3.847	3.962
R_C	3.527	3.347	3.340	3.426	3.293	3.305
ρ_M	113	79	69	104	59	56
ρ_C	58	63	63	57	65	63
CT	49	29	35	29	14	18
$X_{lp}\rightarrow Mp_z^*$	11.4	5.8	9.5	8.3	2.7	5.2

[a]small imaginary frequency of 7i cm^{-1}

[b]small imaginary frequency of 24i cm^{-1}

Another stable minimum located on the potential energy surface of most of these dyads is related to type 3, but the XCCH molecule is rotated around. As may be seen in Fig 3, type 4 places the X atom directly above the M, and promotes a C··C tetrel bond as a secondary interaction. The primary characteristics of these dimers are displayed in Tables 7 and 8. The interaction energies are comparable to, but generally slightly smaller than, the type 3 dimers. Again, one sees the progressive weakening of the interaction with larger metal atom, and with the replacement of I by Cl. R_M is somewhat longer for type 4; some but not all of this difference can be ascribed to the larger radii of Cl and I when compared to C. In a converse relationship, the R_C distances in type 4 are considerably shorter than R_X within type 3.

One distinct difference is the considerably larger total charge transfer in type 4, again reflecting a net transfer from XCCH to the metal system. As may be gleaned from the final row of Tables 7 and 8, this transfer is focused in the overlap between the X lone pairs and the empty p_z orbital of the metal atom. E2 for this transfer is rather large, as high as 17 kcal/mol. While AIM suggests the presence of a reinforcing C··C tetrel bond, NBO places the source of the intermolecular interaction squarely on the metal π-hole bonding. Lastly, the similarity between type 3 and 4 configurations is reiterated in terms of their SAPT energy decomposition. Both the absolute magnitudes, and the proportional contributions, of each of the components are rather similar between types 3 and 4, as is evident by a glance at Table 3. Both are dispersion-dominated with a significant contribution from electrostatics.

It was mentioned above that Ru avoids a type 3 configuration. The same can be said of type 4 to a certain extent. The Ru structures are not true minima, with both ICCH and ClCCH dyads containing a small negative frequency.

SUMMARY AND DISCUSSION

Acting clearly as electron acceptors, the group 10 metals form noncovalent bonds with a NH_3 ligand, highly dependent on charge transfer from the N lone pair to the vacant p_z orbital of the metal. These bond energies diminish quickly, from 10.8 kcal/mol for Ni to only 1.8 kcal/mol for Pt, and the bond elongates, as the metal grows in size and its charge reverses from positive to negative. This charge reversal is accompanied by dramatically lowered electrostatic and induction components. There is also a similar pattern of charge reversal for the corresponding group 8 metals, but this property is largely irrelevant since these metals form a strong and short coordinate covalent M-N bond with NH_3, with interaction energies between 33 and 43 kcal/mol.

Unlike NH_3, a XCCH molecule can engage with the metal system in one of three different configurations. The first places XCCH largely along the axis perpendicular to the metal system. This alignment presents the appearance of a CX··M halogen bond, but detailed examination of the wavefunction suggests this XB represents only a minor contributor to the binding. The major source of the interaction is the charge transfer from the X lone pairs to the π-hole lying above the metal, i.e. its empty p_z orbital. Were these interactions primarily due to halogen bonding, one would expect a strong dependence on the metal and its electrostatic potential, but such is not the case. Indeed, the electrostatic component of the binding is most attractive for Ni, but this metal has a positive MEP so ought to repel the positive σ-hole of the approaching XCCH, as opposed to Pt whose negative charge might be expected to have the largest coulombic attraction. In fact, the electrostatic term is less important than dispersion which is the major contributor to the binding of these configurations. Not all of the metal atoms engage in this configuration with XCCH. For example, Ni and Pd only form such a geometry with ICCH, not ClCCH; Fe and Ru

do not form a stable configuration of this sort at all. The interaction energies of this dimer type lie between 2.2 and 5.0 kcal/mol, higher for ICCH than for ClCCH.

The other two geometry types observed for these pairs place the XCCH roughly parallel to the metal system, in a stacked arrangement. They differ by a rotation of the XCCH, and in the atoms of this unit that bind to those of the metal system. Type 3 places the CH carbon directly above the metal, and its X atom above a C center of the metal complex. It is held together primarily by charge transfer from the C≡C π-bonding orbitals to the empty Mp_z orbital. There is a small supplement arising from transfer between the X lone pairs and SC bonding orbitals within the metal ligand. The XCCH rotation to type 4 places the X atom above the M, and its lone pairs transfer charge into the empty Mp_z orbital. So one can attribute the binding in both of these geometries largely to a TM π-hole bond.

Whether type 3 or 4, dispersion dominates the interaction energy, contributing more than half of the total. This component is followed by the electrostatic term which accounts for between 27% and 37%, with induction a minor player. The group 10 metals form both of these dyads, and with both ICCH and ClCCH. There is a clear pattern of diminishing interaction energy in the Ni > Pd > Pt order. This pattern may be connected to the reversal of metal charge from positive to negative, and the ensuing reduced attraction with the negative regions of XCCH, an idea which is supported by the trends of the ES component.

The group 8 metals form these type 3 and 4 complexes more erratically. For example, Ru does not engage in a type 3 structure at all and its type 4 structures come with a small imaginary frequency. Like their group 10 cousins, the energies of the group 8 metals diminish for lower rows of the periodic table.

It is interesting to compare the energetics of these various dyad types to identify those that would be favored. Ni and Pd both prefer type 3 with type 2 least stable. Indeed, Ni does not form a type 2 structure at all with ClCCH. The situation reverses for Pt where it is the type 2 perpendicular alignment that is favored with ICCH. ClCCH is a different story where type 3 is preferred; in fact the type 2 geometry contains a small imaginary frequency. Group 8 patterns are different. Neither Fe nor Ru engage in a perpendicular structure of type 2. Fe has a clear preference for type 3, with interaction energies around 6 kcal/mol. Os, on the other hand, favors type 2 with ICCH; ClCCH has nearly equal energies for types 2, 3, and 4. Ru is an outlier in the sense that is seems to eschew interactions of any sort with XCCH. Even its type 4 configurations are dubious, with small imaginary frequencies.

It might be noted that several of the dyads reported above contained one small imaginary frequency. As one example, there is a frequency of 4i cm^{-1} type 2 Pt-Cl dimer which pertains to a bending away from a strict perpendicular arrangement of the two subunits. With regard to the type 3 Os-Cl dimer, the 14i frequency refers to a twisting of the two molecules, retaining their stacked parallel arrangement. Several of the type 4 geometries of the group 8 metals were also characterized by small imaginary frequencies. For both Ru-Cl and Os-Cl, the mode involves a bending of the metal monomer unit away from planarity. In the case of Ru-I, the 24i cm^{-1} mode involves a combined twist and turn of the two subunits with respect to one another. In no case was this phenomenon caused by externally imposed symmetry as no such restriction was imposed. In all cases, if a geometry optimization was begun with a structure consistent with deformations of this type, the system simply bounced back to the original starting point whose data are contained in the tables. As one last comparative point, the interaction energies of several dyads computed here via the M06-2X functional were recalculated using ωB97X-D. There was little change noticed, with quantities within 1 kcal/mol of each other, sometimes even closer.

An earlier study [74] had noted that I atoms might approach a Ni within a square planar arrangement closer than their vdW radii sum, and the accompanying survey of the CCSD had yielded some 50 crystal structures of this sort where Ni lies close to a halogen or O atom. Bikbaeva christened such noncovalent bonding to a transition metal as semicoordination, a term which has found wider use over the years [97, 98]. Their AIM calculations found BCP densities of roughly 0.01 au but they did not perform the calculations necessary to elucidate the orbitals involved or the direction of charge transfer. They were therefore unable to distinguish halogen from semicoordination bonding.

Several years thereafter, calculations were completed [76] that involve the full Ni,Pd,Pt set of group 10 metals in a square planar setting. The MEP charges on these centers were manipulated by various substitutions so as to cover both positive and negative values. Pyridine and pentafluoroidobenzene were paired with these metal systems as potential electron donor and acceptor, respectively. Stable complexes were found whether the metal carried a partial positive or negative charge. In agreement with the systems examined here, the potential above the Ni atom tended to be more positive than Pd, which was in turn more positive than Pt. Also consistent is the ordering of the type 1 interaction energies as Ni > Pd > Pt, in this case pyridine rather than NH_3. As another point of agreement with experiment, a crystal study [73] found a nonlinear CI··N angle of 143° when square planar (nitrosoguanidinate)Ni was paired with 1,3,5-triiodotrifluorobenzene.

As in the perpendicular type 2 geometries examined here, interaction energies were largely insensitive to the identity of the metal center. The authors noted a NBO charge transfer from the M lone pair to the σ*(CI) orbitals of the iodobenzene derivative, which fit with the authors' supposition of halogen bonding. Notably, the E2 quantities for this transfer were rather small, particularly when the M was surrounded by 4 S-ligands as in the systems studied here. However, this work did not consider charge transfers in the opposite direction, from the I lone pairs to the metal system, which were found here to be much larger, so the characterization of these interactions as primarily halogen bonding was premature. More recent calculations [77] have focused on the 3d set of transition metal atoms Co, Ni, Cu and Zn, ensconced within a porphyrin framework. This work nicely confirms the findings presented here of a strong element of charge transfer from the halogen lone pairs to the empty metal p_z orbital, which would classify these interactions as metal π-hole semicoordination, rather than halogen bonds.

It might be emphasized that the results here apply strictly to the intrinsic bonding preferences of these systems, calculated *in vacuo* in the absence of surrounding molecules. When placed within a crystal environment, the interactions with other units as well as other sorts of crystal packing forces, might easily influence the geometries observed. So for example, the relatively small energy differences between some of the types 2, 3, and 4 geometries could easily be overwhelmed by these external influences. As another consideration, the absence of minima for certain configurations in the gas phase, for example perpendicular type 2 complexes for Ru and Os, certainly does not rule out their appearance within a crystal. Indeed, if such geometries were to occur, they could certainly contain elements of M··X bonding, along with other intermolecular attractive forces that would be present.

CONCLUSIONS

Despite similarities in their overall electronic structure and surrounding electrostatic potentials, the group 8 and 10 metal atoms behave quite differently in connection with an approaching ligand. Most dramatically, the Fe/Ru/Os series form a short strong, largely covalent

bond with NH_3, between 33 and 44 kcal/mol. The bonds with the group 10 metals are much longer and weaker, dropping from 11 kcal/mol for Ni down to only 2 kcal/mol for Pt.

Response to an approaching XCCH unit is quite variable. In one configuration, the XCCH aligns itself directly above the M center, perpendicular to the metal system. These interaction energies lie in the 2-5 kcal/mol range. Neither Fe nor Ru participate in such a configuration, and ClCCH only forms such a dyad with the Pt system. These interactions are comprised largely of a charge transfer from the X lone pair to the π-hole above the M, with only a smaller component of halogen bonding.

The last category of geometry places the XCCH above and nearly parallel to the metal system. In one variant, type 3, one of the C atoms lies above the M, while the X is located above M in type 4. In either case, the primary bonding involves electron donation to the unoccupied p_z orbital of the metal center. Type 3 configurations are preferred energetically for most of the group 10 metals, with the exception of Pt/ICCH, which favors the perpendicular arrangement. While Ru eschews a parallel dyad, both Fe and Os participate and that involving Fe is particularly strong, with a binding energy of some 6 kcal/mol, twice that of Os. The binding energies of the parallel structures diminish as the central metal atom is enlarged.

Regardless of the geometry adopted by each dyad, whether perpendicular or parallel, the primary element of the bonding is a semicoordinate transition metal bond, in which the M center serves as the primary electron acceptor. It would thus behoove future researchers to examine the electronic structure in some detail so as to more accurately characterize the nature of the bonding in these and related complexes.

Acknowledgments

This material is based upon work supported by the U.S. National Science Foundation under Grant No. 1954310.

Conflicts of interest

There are no conflicts to declare.

REFERENCES

1. M. D. Joesten and L. J. Schaad, *Hydrogen Bonding*, Marcel Dekker, New York, 1974.
2. E. Arunan, G. R. Desiraju, R. A. Klein, J. Sadlej, S. Scheiner, I. Alkorta, D. C. Clary, R. H. Crabtree, J. J. Dannenberg, P. Hobza, H. G. Kjaergaard, A. C. Legon, B. Mennucci and D. J. Nesbitt, *Pure Appl. Chem.*, 2011, **83**, 1637-1641.
3. S. J. Grabowski, ed. *Hydrogen Bonding - New Insights*, Springer, Dordrecht, Netherlands, 2006.
4. A. Chand, D. K. Sahoo, A. Rana, S. Jena and H. S. Biswal, *Acc. Chem. Res.*, 2020, **53**, 1580-1592.
5. S. Scheiner and L. Wang, *J. Am. Chem. Soc.*, 1993, **115**, 1958-1963.
6. H. S. Biswal and S. Wategaonkar, *J. Chem. Phys.*, 2011, **135**, 134306.
7. M. Cuma, S. Scheiner and T. Kar, *J. Mol. Struct. (Theochem)*, 1999, **467**, 37-49.
8. S. M. Cybulski and S. Scheiner, *Chem. Phys. Lett.*, 1990, **166**, 57-64.
9. S. Scheiner and X. Duan, *Phys. Chem. Chem. Phys.*, 1991, **60**, 874-883.

10. J. E. Del Bene, I. Alkorta, G. Sanchez-Sanz and J. Elguero, *J. Phys. Chem. A*, 2011, **115**, 13724-13731.
11. S. Scheiner and J. Lu, *Chem. Eur. J.*, 2018, **24**, 8167-8177.
12. A. Bauzá, D. Quiñonero, A. Frontera and P. M. Deyà, *Phys. Chem. Chem. Phys.*, 2011, **13**, 20371-20379.
13. V. d. P. N. Nziko and S. Scheiner, *J. Org. Chem.*, 2015, **80**, 2356-2363.
14. W. Dong, Q. Li and S. Scheiner, *Molecules*, 2018, **23**, 1681.
15. A. Bauzá, T. J. Mooibroek and A. Frontera, *Angew. Chem. Int. Ed.*, 2013, **52**, 12317-12321.
16. S. J. Grabowski, *J. Phys. Chem. A*, 2011, **115**, 12340-12347.
17. S. J. Grabowski, *Phys. Chem. Chem. Phys.*, 2014, **16**, 1824-1834.
18. Z. P. Shields, J. S. Murray and P. Politzer, *Int. J. Quantum Chem.*, 2010, **110**, 2823-2832.
19. G. Chalasinski, S. M. Cybulski, M. M. Szczesniak and S. Scheiner, *J. Chem. Phys.*, 1989, **91**, 7809-7817.
20. P. Politzer, J. S. Murray and Z. Peralta-Inga, *Int. J. Quantum Chem.*, 2001, **85**, 676-684.
21. T. Clark, M. Hennemann, J. S. Murray and P. Politzer, *J. Mol. Model.*, 2007, **13**, 291-296.
22. J. S. Murray, P. Lane, T. Clark, K. E. Riley and P. Politzer, *J. Mol. Model.*, 2012, **18**, 541-548.
23. A. Bauzá, R. Ramis and A. Frontera, *J. Phys. Chem. A*, 2014, **118**, 2827-2834.
24. V. d. P. N. Nziko and S. Scheiner, *Phys. Chem. Chem. Phys.*, 2016, **18**, 3581-3590.
25. W. Zierkiewicz, M. Michalczyk and S. Scheiner, *Phys. Chem. Chem. Phys.*, 2018, **20**, 4676-4687.
26. S. Scheiner, *J. Phys. Chem. A*, 2021, **125**, 6514-6528.
27. D. Jovanovic, M. Poliyodath Mohanan and S. M. Huber, *Angew. Chem. Int. Ed.*, 2024, **63**, e202404823.
28. Q. Zhang, Y.-Y. Chan, M. Zhang, Y.-Y. Yeung and Z. Ke, *Angew. Chem. Int. Ed.*, 2022, **61**, e202208009.
29. Y. Lu, Q. Liu, Z.-X. Wang and X.-Y. Chen, *Angew. Chem. Int. Ed.*, 2022, **61**, e202116071.
30. R. Hein, A. Docker, J. J. Davis and P. D. Beer, *J. Am. Chem. Soc.*, 2022, **144**, 8827-8836.
31. A. Docker, X. Shang, D. Yuan, H. Kuhn, Z. Zhang, J. J. Davis, P. D. Beer and M. J. Langton, *Angew. Chem. Int. Ed.*, 2021, **60**, 19442-19450.
32. J. Zhang, A. Hao and P. Xing, *Chem. Eur. J.*, 2024, **30**, e202401004.
33. Z. Wang, Z. Cao, A. Hao and P. Xing, *Chem. Sci.*, 2024, **15**, 6924-6933.
34. T.-N. Streit, R. M. Gomila, R. Sievers, A. Frontera and M. Malischewski, *CrystEngComm*, 2024, **26**, 594-598.
35. R. Tian, Y. Zeng, X. Li and X. Zhang, *New J. Chem.*, 2024, **48**, 6582-6589.
36. R. M. Gomila, E. R. T. Tiekink and A. Frontera, *Inorganics*, 2023, **11**, 468.
37. P. Middya, M. Karmakar, R. M. Gomila, M. G. B. Drew, A. Frontera and S. Chattopadhyay, *New J. Chem.*, 2023, **47**, 9346-9363.
38. Q. Yang, Q. Wu, X. Zhang, X. Yang and Q. Li, *Mol. Phys.*, 2022, **120**, e2102548.
39. M. Jabłoński, *Molecules*, 2021, **26**, 2275.
40. R. Llull, G. Montalbán, I. Vidal, R. M. Gomila, A. Bauzá and A. Frontera, *Phys. Chem. Chem. Phys.*, 2021, **23**, 16888-16896.
41. R. M. Gomila, A. Bauzá, T. J. Mooibroek and A. Frontera, *CrystEngComm*, 2021, **23**, 3084-3093.

42. A. Bauzá, I. Alkorta, J. Elguero, T. J. Mooibroek and A. Frontera, *Angew. Chem. Int. Ed.*, 2020, **59**, 17482-17487.
43. S. Burguera, A. Bauzá and A. Frontera, *Phys. Chem. Chem. Phys.*, 2024, **26**, 16550-16560.
44. J. Yan, Y. Zeng, L. Meng, X. Li and X. Zhang, *Phys. Chem. Chem. Phys.*, 2023, **25**, 29155-29164.
45. J. Li, Q. Feng, C. Wang and Y. Mo, *Phys. Chem. Chem. Phys.*, 2023, **25**, 15371-15381.
46. M. de las Nieves Piña, T. J. Mooibroek, A. Frontera and A. Bauzá, *Phys. Chem. Chem. Phys.*, 2022, **24**, 24983-24991.
47. A. Pizzi, M. Calabrese, A. Daolio, M. Ursini, A. Frontera and G. Resnati, *CrystEngComm*, 2022, **24**, 3846-3851.
48. A. Shan, X. Li, Y. Zeng, L. Meng and X. Zhang, *New J. Chem.*, 2022, **46**, 3315-3324.
49. G. Sánchez-Sanz, C. Trujillo, I. Alkorta and J. Elguero, *ChemPhysChem.*, 2020, **21**, 2557-2563.
50. R. Wang, Z. Wang, X. Yu and Q. Li, *ChemPhysChem.*, 2020, **21**, 2426-2431.
51. A. Daolio, A. Pizzi, M. Calabrese, G. Terraneo, S. Bordignon, A. Frontera and G. Resnati, *Angew. Chem. Int. Ed.*, 2021, **60**, 20723-20727.
52. M. Calabrese, A. Pizzi, A. Daolio, R. Beccaria, C. Lo Iacono, S. Scheiner and G. Resnati, *Chem. Eur. J.*, 2024, **30**, e202304240.
53. S. Burguera, R. M. Gomila, A. Bauzá and A. Frontera, *Cryst.*, 2023, **13**, 187.
54. S. Burguera, A. K. Sahu, M. J. Chávez Romero, H. S. Biswal and A. Bauzá, *Phys. Chem. Chem. Phys.*, 2024, **26**, 18606-18613.
55. D. Grödler, S. Burguera, A. Frontera and E. Strub, *Chem. Eur. J.*, 2024, **30**, e202400100.
56. Y. Xu, M. Calabrese, N. Demitri, A. Pizzi, T. Nag, I. Hung, Z. Gan, G. Resnati and D. L. Bryce, *Chem. Commun.*, 2023, **59**, 12609-12612.
57. I. Alkorta, J. Elguero and A. Frontera, *Cryst.*, 2020, **10**, 180.
58. A. Bauzá and A. Frontera, *Chem. Eur. J.*, 2022, **28**, e202201660.
59. M. Michalczyk, W. Zierkiewicz and S. Scheiner, *Phys. Chem. Chem. Phys.*, 2024, **26**, 5836-5847.
60. M. Calabrese, R. M. Gomila, A. Pizzi, A. Frontera and G. Resnati, *Chem. Eur. J.*, 2023, **29**, e202302176.
61. G. Li, J. H. Stenlid, M. S. G. Ahlquist and T. Brinck, *J. Phys. Chem. C*, 2020, **124**, 14696-14705.
62. J. H. Stenlid and T. Brinck, *J. Am. Chem. Soc.*, 2017, **139**, 11012-11015.
63. T. Brinck and J. H. Stenlid, *Advanced Theory and Simulations*, 2019, **2**, 1800149.
64. J. H. Stenlid, A. J. Johansson and T. Brinck, *Cryst.*, 2017, **7**, 222.
65. Z. Shen, X. Li, Y. Zeng and X. Zhang, *J. Phys. Chem. A*, 2024, **128**, 10796-10807.
66. A. V. Rozhkov, E. Y. Tupikina, K. I. Tugashov and V. Y. Kukushkin, *CrystEngComm*, 2024, **26**, 5607-5616.
67. A. V. Rozhkov, S. Burguera, A. Frontera and V. Y. Kukushkin, *Cryst. Growth Des.*, 2024, **24**, 9581-9589.
68. L. de Azevedo Santos, T. Wagner, K. Visscher, J. Nitsch, F. M. Bickelhaupt and C. Fonseca Guerra, *Phys. Chem. Chem. Phys.*, 2024, **26**, 20928-20936.
69. A. M. Cheranyova, L. E. Zelenkov, S. V. Baykov, Y. A. Izotova, D. M. Ivanov, N. A. Bokach and V. Y. Kukushkin, *Inorg. Chem.*, 2024.

70. S. V. Baykov, E. A. Katlenok, S. O. Baykova, A. V. Semenov, N. A. Bokach and V. P. Boyarskiy, *Int. J. Mol. Sci.*, 2024, **25**, 4052.
71. S. Burguera, A. Bauzá and A. Frontera, *ChemPhysChem.*, 2023, **24**, e202300585.
72. C. Zhang, H. Bai, J. Hu, K. Guo and L. Zhao, *J. Comput. Chem.*, 2023, **44**, 480-488.
73. D. M. Ivanov, N. A. Bokach, V. Yu. Kukushkin and A. Frontera, *Chem. Eur. J.*, 2022, **28**, e202103173.
74. Z. M. Bikbaeva, D. M. Ivanov, A. S. Novikov, I. V. Ananyev, N. A. Bokach and V. Y. Kukushkin, *Inorg. Chem.*, 2017, **56**, 13562-13578.
75. L. E. Zelenkov, A. A. Eliseeva, S. V. Baykov, V. V. Suslonov, B. Galmés, A. Frontera, V. Y. Kukushkin, D. M. Ivanov and N. A. Bokach, *Inorganic Chemistry Frontiers*, 2021, **8**, 2505-2517.
76. S. Burguera, A. Bauzá and A. Frontera, *Int. J. Mol. Sci.*, 2023, **24**, 15597.
77. R. Siddiqui, S. Burguera, M. de las Nieves Piña, S. Dhamija, H. M. Titi, A. Frontera, A. Bauzá and R. Patra, *Angew. Chem. Int. Ed.*, 2024, **63**, e202409963.
78. Gaussian 16 Rev. C.01, M. J. Frisch, G. W. Trucks, H. B. Schlegel, G. E. Scuseria, M. A. Robb, J. R. Cheeseman, G. Scalmani, V. Barone, G. A. Petersson, H. Nakatsuji, X. Li, M. Caricato, A. V. Marenich, J. Bloino, B. G. Janesko, R. Gomperts, B. Mennucci, H. P. Hratchian, J. V. Ortiz, A. F. Izmaylov, J. L. Sonnenberg, D. Williams-Young, F. Ding, F. Lipparini, F. Egidi, J. Goings, B. Peng, A. Petrone, T. Henderson, D. Ranasinghe, V. G. Zakrzewski, J. Gao, N. Rega, G. Zheng, W. Liang, M. Hada, M. Ehara, K. Toyota, R. Fukuda, J. Hasegawa, M. Ishida, T. Nakajima, Y. Honda, O. Kitao, H. Nakai, T. Vreven, K. Throssell, J. A. Montgomery Jr., J. E. Peralta, F. Ogliaro, M. J. Bearpark, J. J. Heyd, E. N. Brothers, K. N. Kudin, V. N. Staroverov, T. A. Keith, R. Kobayashi, J. Normand, K. Raghavachari, A. P. Rendell, J. C. Burant, S. S. Iyengar, J. Tomasi, M. Cossi, J. M. Millam, M. Klene, C. Adamo, R. Cammi, J. W. Ochterski, R. L. Martin, K. Morokuma, O. Farkas, J. B. Foresman and D. J. Fox, 2016, Gaussian, Inc, Wallingford, CT.
79. Y. Zhao and D. G. Truhlar, *Theor. Chem. Acc.*, 2008, **120**, 215-241.
80. G. Paytakov, T. Dinadayalane and J. Leszczynski, *J. Phys. Chem. A*, 2015, **119**, 1190-1200.
81. B. S. D. R. Vamhindi and A. Karton, *Chem. Phys.*, 2017, **493**, 12-19.
82. R. Podeszwa and K. Szalewicz, *J. Chem. Phys.*, 2012, **136**, 161102.
83. S. Karthikeyan, V. Ramanathan and B. K. Mishra, *J. Phys. Chem. A*, 2013, **117**, 6687-6694.
84. M. Majumder, B. K. Mishra and N. Sathyamurthy, *Chem. Phys.*, 2013, **557**, 59-65.
85. M. A. Vincent and I. H. Hillier, *Phys. Chem. Chem. Phys.*, 2011, **13**, 4388-4392.
86. A. D. Boese, *ChemPhysChem.*, 2015, **16**, 978-985.
87. M. Walker, A. J. A. Harvey, A. Sen and C. E. H. Dessent, *J. Phys. Chem. A*, 2013, **117**, 12590-12600.
88. L. F. Molnar, X. He, B. Wang and K. M. Merz, *J. Chem. Phys.*, 2009, **131**, 065102.
89. S. F. Boys and F. Bernardi, *Mol. Phys.*, 1970, **19**, 553-566.
90. T. Lu and F. Chen, *J. Comput. Chem.*, 2012, **33**, 580-592.
91. AIMAll, T. A. Keith, 2013, TK Gristmill Software, Overland Park KS.
92. A. E. Reed and F. Weinhold, *J. Chem. Phys.*, 1983, **78**, 4066-4073.
93. A. E. Reed, F. Weinhold, L. A. Curtiss and D. J. Pochatko, *J. Chem. Phys.*, 1986, **84**, 5687-5705.

94. K. Szalewicz and B. Jeziorski, in *Molecular Interactions. From Van der Waals to Strongly Bound Complexes*, ed. S. Scheiner, Wiley, New York1997, pp. 3-43.
95. K. Szalewicz and B. Jeziorski, *J. Mol. Model.*, 2022, **28**, 273.
96. D. G. A. Smith, L. A. Burns, A. C. Simmonett, R. M. Parrish, M. C. Schieber, R. Galvelis, P. Kraus, H. Kruse, R. D. Remigio, A. Alenaizan, A. M. James, S. Lehtola, J. P. Misiewicz, M. Scheurer, R. A. Shaw, J. B. Schriber, Y. Xie, Z. L. Glick, D. A. Sirianni, J. S. O'Brien, J. M. Waldrop, A. Kumar, E. G. Hohenstein, B. P. Pritchard, B. R. Brooks, H. F. SchaeferIII, A. Y. Sokolov, K. Patkowski, A. E. DePrinceIII, U. Bozkaya, R. A. King, F. A. Evangelista, J. M. Turney, T. D. Crawford and C. D. Sherrill, *J. Chem. Phys.*, 2020, **152**, 184108.
97. L. E. Zelenkov, D. M. Ivanov, E. K. Sadykov, N. A. Bokach, B. Galmés, A. Frontera and V. Y. Kukushkin, *Cryst. Growth Des.*, 2020, **20**, 6956-6965.
98. L. G. Fachini, G. B. Baptistella, K. Postal, F. S. Santana, E. M. de Souza, R. R. Ribeiro, G. G. Nunes and E. L. Sá, *RSC Advances*, 2023, **13**, 27997-28007.

Data Availability

Data are available upon request from the author.